







Observation of near-infrared sub-Poissonian photon emission in hexagonal boron nitride at room temperature

Cite as: APL Photonics 5, 076103 (2020); <https://doi.org/10.1063/5.0008242>

Submitted: 19 March 2020 . Accepted: 21 June 2020 . Published Online: 07 July 2020

Robin Camphausen , Loris Marini , Sherif Abdulkader Tawfik , Toan Trong Tran , Michael J. Ford , and Stefano Palomba 



View Online



Export Citation



CrossMark

ARTICLES YOU MAY BE INTERESTED IN

[Atomistic defects as single-photon emitters in atomically thin MoS₂](#)

Applied Physics Letters **117**, 070501 (2020); <https://doi.org/10.1063/5.0018557>


[Invited Review Article: Single-photon sources and detectors](#)

Review of Scientific Instruments **82**, 071101 (2011); <https://doi.org/10.1063/1.3610677>

[Amorphous superconducting nanowire single-photon detectors integrated with nanophotonic waveguides](#)

APL Photonics **5**, 076106 (2020); <https://doi.org/10.1063/5.0004677>

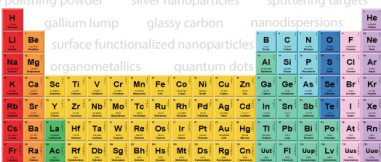
additive manufacturing epitaxial crystal growth cerium oxide polishing powder silver nanoparticles sputtering targets



THE ADVANCED MATERIALS MANUFACTURER®

deposition slugs OLED Lighting spintronics solar energy osmium nanoribbons thin films chalcogenides AuNPs GDC li-ion battery electrolytes 99.999% ruthenium spheres

endohedral fullerenes copper nanoparticles diamond micropowder CIGS MBE grade materials palladium catalysts flexible electronics beta-barium borate borosilicate glass dysprosium pellets YBCO pyrolytic graphite 3d graphene foam indium tin oxide mesoporous silica raman substrates sapphire windows tungsten carbide InGaAs barium fluoride carbon nanotubes lithium niobate scandium powder



gallium lump glassy carbon nanodispersions III-IV semiconductors CVD precursors europium phosphors InAs wafers laser crystals ultra high purity materials MOFs rare earth metals photovoltaics refractory metals MOCVD organometallics quantum dot superconductors transparent ceramics ultra high purity silicon

*American Elements opens up a world of possibilities so you can **Now Invent!***

Over 15,000 certified high purity laboratory chemicals, metals, & advanced materials and a state-of-the-art Research Center. Printable GHS-compliant Safety Data Sheets. Thousands of new products. And much more. All on a secure multi-language "Mobile Responsive" platform.

perovskite crystals yttrium iron garnet alternative energy h-BN gold nanocubes graphene oxide macromolecules photonics rhodium sponge fiber optics beamsplitters infrared dyes zeolites fused quartz metallocenes platinum ink buckyballs Ti-6Al-4V

Now Invent.™
The Next Generation of Material Science Catalogs

www.americanelements.com

Observation of near-infrared sub-Poissonian photon emission in hexagonal boron nitride at room temperature

Cite as: APL Photon. 5, 076103 (2020); doi: 10.1063/5.0008242

Submitted: 19 March 2020 • Accepted: 21 June 2020 •

Published Online: 7 July 2020



View Online



Export Citation



CrossMark

Robin Camphausen,^{1,2}  Loris Marini,^{1,2}  Sherif Abdulkader Tawfik,³  Toan Trong Tran,⁴ 
Michael J. Ford,⁴  and Stefano Palomba^{1,2,a)} 

AFFILIATIONS

¹Institute of Photonics and Optical Science (IPOS), The University of Sydney, Sydney, NSW 2006, Australia

²The University of Sydney Nano Institute, The University of Sydney, Sydney, NSW 2006, Australia

³School of Science, RMIT University, GPO Box 2476, Melbourne, Victoria 3001, Australia

⁴School of Mathematical and Physical Sciences, University of Technology Sydney, Ultimo, New South Wales 2007, Australia

^{a)} Author to whom correspondence should be addressed: stefano.palomba@sydney.edu.au

ABSTRACT

The generation of non-classical light states in the near-infrared (NIR) is important for a number of photonic quantum technologies. Here, we report the first experimental observation of sub-Poissonian NIR (1.24 eV) light emission from defects in a 2D hexagonal boron nitride (hBN) sheet at room temperature. Photoluminescence statistics shows $g^{(2)}(0) = 0.6$, which is a signature of the quantum nature of the emission. Density functional-theory calculations, at the level of the generalized gradient approximation, for the negatively charged nitrogen anti-site lattice defects are consistent with the observed emission energy. This work demonstrates that the defects in hBN could be a promising platform for single-photon generation in the NIR.

© 2020 Author(s). All article content, except where otherwise noted, is licensed under a Creative Commons Attribution (CC BY) license (<http://creativecommons.org/licenses/by/4.0/>). <https://doi.org/10.1063/5.0008242>

I. INTRODUCTION

It is well-known that coherent light is the most stable classical light achievable, which exhibits a Poissonian statistical distribution. Shot noise represents the limit of this intrinsic randomness associated with the time separation of photons emitted using a Poissonian light source. Therefore, a more regular, or sub-Poissonian, stream of photons reveals the quantum nature of the underlying radiative process.¹ A perfectly regular light source, where no more than one photon is emitted at any given time, is known as a single-photon source (SPS) and represents an essential building block for a variety of quantum technologies, including quantum computation schemes, boson sampling, precision metrology, as well as secure communication applications, such as quantum key distribution.^{2–6}

An ideal SPS would provide high-brightness, high-purity, indistinguishable photons at room temperature while being integrable and reliable to fabricate.^{6,7} Moreover, it is desirable for the

emission to be in the near-infrared (NIR) wavelength range in order to facilitate a seamless integration with modern optical communication platforms.⁸ Though much progress has been made toward this goal on a number of platforms, the design of an ideal SPS remains elusive. Gallium and indium based quantum dots can currently provide high-brightness single-photon emission (SPE) in the NIR with unrivalled purity among other SPSs and indistinguishability, but require cumbersome cooling equipment to operate at cryogenic temperatures.^{8–11} Localized defects in gallium nitride and color-centers in single-walled carbon nanotubes were shown to emit single photons across the visible and NIR spectrum,^{12,13} with recent results including electrically driven light emission¹⁴ and room temperature SPE in the NIR.^{15,16} However, spectral purity is poor and fabrication remains challenging.¹⁷

Recently, two-dimensional van der Waals (vdW) crystals, such as transition metal dichalcogenides (TMDCs) and hexagonal boron nitride (hBN), have emerged as an attractive platform for SPE.¹⁸ SPE

was observed at cryogenic temperatures from TMDCs, where quantum defects are ascribed to localized, weakly bound excitons.¹⁹ On the other hand, some lattice defects in hBN are located deep within the bandgap, giving rise to states that allow bright, room temperature SPE; a discovery that has prompted extensive investigation in recent years into the use of hBN in particular in quantum photonics.^{18,20–22} SPE from hBN has now been demonstrated over a large range of wavelengths in the visible as well as ultraviolet.^{23,24} One advantage of using vdW materials is that due to their quantum-confined nature all emitters are localized on a surface, facilitating light collection and enhancement through the use of fibers or antennas.^{25–27} Active research in new fabrication methods complements well-established and scalable techniques, enabling fine control over material parameters and geometries. Recent developments include bottom-up fabrication, self-assembly of vdW crystals on nanoparticles, and the deterministic creation of SPE defects through the use of nano-patterning on hBN.^{28–31} Moreover, it has been shown that the emission wavelength from hBN SPSSs can be tuned by the application of a mechanical strain or electrical bias.^{32,33} A recent study using simultaneous optical and electron microscopy imaging of a number of visible wavelength SPSSs in hBN has been a significant step toward systematically identifying the effect of strain and local electronic interactions on the emission spectrum.³⁴ The observation that hBN SPE defects possess an intrinsic spin that can be optically controlled and read out further enhances the attractiveness of hBN for quantum photonic applications.³⁵

Here, we present the first room temperature observation of sub-Poissonian emission in the NIR from hBN. This is demonstrated by the measurement of the second-order correlation function $g^{(2)}(0) < 1$ on the emission. In order to understand the origin of the emission, we apply density functional-theory (DFT) to calculate the electronic properties of various defects in the hBN lattice. We attribute this emission at 1.24 eV (998 nm) to the negatively charged nitrogen anti-site defect ($V_N N_B^{-1}$).

II. METHOD

Multilayer hBN flakes were obtained commercially and annealed at high temperature in an inert environment to activate the quantum emitters (details about the sample fabrication can be found in the [supplementary material](#)). Samples were imaged using

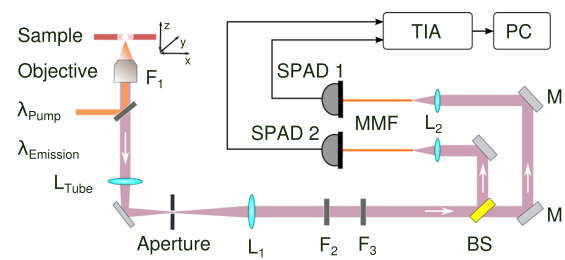


FIG. 1. Experimental setup of a free-space HBT interferometer for the measurement of $g^{(2)}(\tau)$ in hBN, composed of a beam splitter (BS), a pair of NIR single-photon avalanche photodiodes (SPAD), a time-interval analyzer (TIA), and a personal computer (PC) for time-tagging and processing. A pair of lenses (L_1 , L_2) acts as a telescope to achieve a 1:1 mapping between the image plane and the core of multi-mode fibers (MMF). Confocality is achieved with a small aperture at the focal plane of the tube lens L_{TUBE} and the excitation pump is removed using long-pass filter F_2 . Background light is reduced using short-pass filter F_3 .

a custom-built laser scanning confocal microscope, where 80 MHz, ~ 200 fs pulses at 800 nm wavelength were used as an excitation pump, and NIR-sensitive InGaAs single photon avalanche diodes (SPAD) as detectors. Photoluminescence (PL) was collected directly using a spectrometer or using a Hanbury Brown–Twiss (HBT) interferometer where photon anti-bunching was recorded thanks to a digital time card. These data were then used to calculate the second-order coherence as a function of interphoton delay $g^{(2)}(\tau)$. [Figure 1](#) shows a diagram of the set-up and the detailed experimental method is presented in the [supplementary material](#).

III. RESULTS

A representative confocal scan of a $50 \times 50 \mu\text{m}^2$ sample area is shown in [Fig. 2\(a\)](#), where a number of emitters are visible with light collected at wavelengths above 850 nm (inset: the emitter showing sub-Poissonian photon statistics). The PL spectrum from a non-classical emitter with a center wavelength at 998 nm is displayed in [Fig. 2\(b\)](#). The quantum nature of this emitter is confirmed by the corresponding calculation of the second-order correlation function $g^{(2)}(0) = 0.6 \pm 0.05$, as shown in [Fig. 3\(a\)](#). No background emission

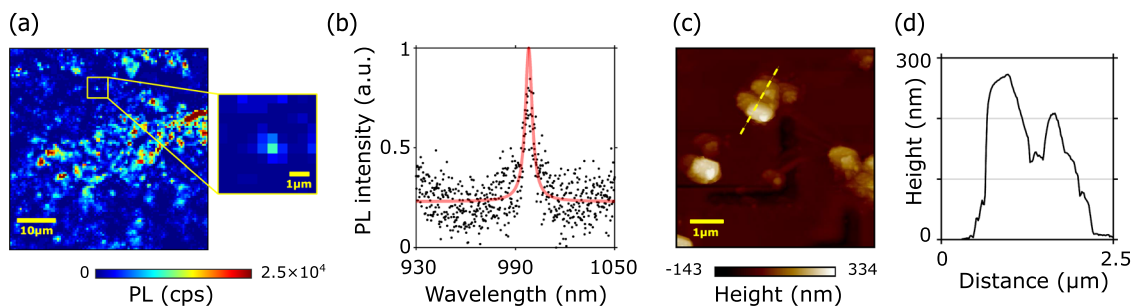


FIG. 2. (a) Confocal map of a hBN sample showing a number of emitters with PL at wavelengths longer than 850 nm. Inset: emitter with sub-Poissonian photon statistics. (b) PL spectra of the sub-Poissonian emitter, with emission centered at 998 nm. Dots are experimental data and solid line is a Lorentzian fit with FWHM 5 nm. (c) AFM image showing several hBN flakes on the sample. (d) Height profile of hBN flake, profile along yellow dotted line shown in (c).

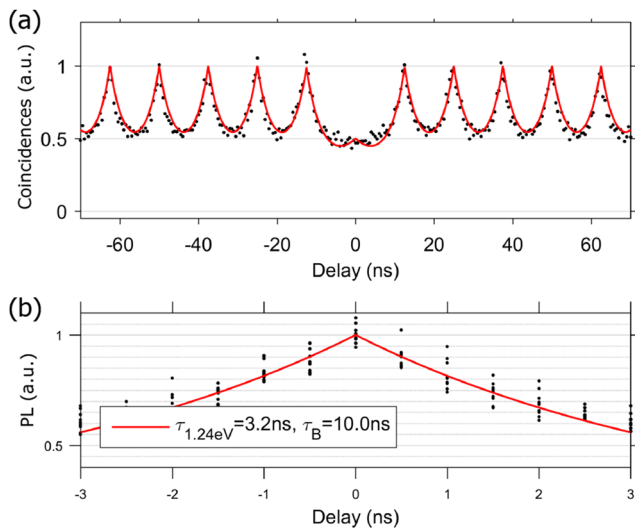


FIG. 3. (a) Second-order coherence function $[g^{(2)}(\tau)]$ of PL emission from the emitter at a wavelength 998 nm (1.24 eV). Dots are experimental data and the solid curve is numerically calculated (procedure described in Sec. III). (b) Emitter lifetime and background level parameters fitting using Eq. (1). Dots are the experimental $\tau \neq 0$ ns peaks from Fig. 3(a), while the solid line is a fit. Lifetimes: $\tau_{1.24 \text{ eV}} = 3.2$ ns and $\tau_B = 10$ ns for SPE and background, respectively, and background level: $B = 0.48$.

was subtracted and the collection time for the displayed $g^{(2)}$ plot was four hours, where the collected photon detection rate was $\sim 11 \times 10^3$ counts/s with an average pump power of 0.7 mW. Accounting for 20% detector quantum efficiency and the optical losses in the setup, we estimate an emission rate of $\sim 1.3 \times 10^6$ counts/s at the sample plane. The typical thickness and lateral diameter of the hBN flakes used are ~ 250 nm and 900 nm, respectively. This can be seen in Figs. 2(c) and 2(d), which show an AFM image and a height profile of typical hBN flakes.

As the emitter was probed with a femtosecond pulsed laser, we can extract the emitter lifetime from peak widths of the experimentally measured $g^{(2)}$ function. We model the SPE as a two-level system with a characteristic decay parameter $\tau_{1.24 \text{ eV}}$ that describes the lifetime of the excited state. In order to account for the observation of a non-zero value $g^{(2)}$ at $\tau = 0$, we further model the background PL as classical light also generated by the pump laser, with a different exponential decay time τ_B . The PL emission flux due to a single excitation pulse can, therefore, be modeled as³⁶

$$p_{em}(t) = e^{-t/\tau_{1.24\text{eV}}} + B e^{-t/\tau_B}, \quad (1)$$

where t is the time after excitation, and B is the relative intensity of the background emission. In order to fit parameters $\tau_{1.24 \text{ eV}}$, τ_B , and B , we note that for an interphoton delay far from 0, the second-order coherence functions of quantum and classical light are equal.¹ We can, therefore, fit Eq. (1) to the $\tau \neq 0$ peaks of the experimentally measured $g^{(2)}$ (2), where now the fitting parameters simply correspond to the decay lifetimes and relative intensities of two classical emitters (see Fig. 3(b) for the fitting). We find a background level $B = 0.48$ and decay lifetimes of $\tau_{1.24 \text{ eV}} = 3.2$ ns for the defect

emission and $\tau_B = 10$ ns for the background. We numerically calculate the full second order correlation function for PL from a quantum emitter and classical background under 80 MHz pulsed excitation. Using the lifetime and background parameters obtained from fitting Eq. (1), we obtain excellent agreement with the experimentally measured coincidences [see Fig. 3(a)], where the observed decay lifetime parameter $\tau_{1.24 \text{ eV}} = 3.2$ ns falls well within the range of previously observed decays from other lattice defect emitters in hBN.^{23,32} The observed background could originate from PL generated within the quartz substrate, or from nearby defects in the hBN lattice. Since the former tends to exhibit very small lifetimes,³⁷ the background is likely to result from a large number of incoherent radiative emissions from other areas of the illuminated hBN lattice.

IV. THEORY

We apply density functional theory (DFT) and constrained-DFT (CDFT) within the generalized gradient approximation using exclusively the Perdew, Burke, and Ernzerhof (PBE) functional to calculate ground and excited states and compare these calculations with the observed NIR SPE from hBN. DFT and CDFT allow us to calculate the coupling between the electronic and vibronic states known as the Huang–Rhys (HR) factor, as well as the energy of the transitions to the ground state and the energy of the zero-phonon-line (ZPL). The HR factor is calculated by applying the one-dimensional (1D) configuration coordinate formulation, where the atomic degrees of freedom are represented by a single coordinate, the configuration coordinate Q . The PL spectral function $L(\hbar\omega)$ is obtained following the generating function procedure,^{38–40} and the electron–phonon spectral function, $S(\hbar\omega)$, and the partial HR factor S_k are derived according to the procedure outlined in Ref. 21. The width of the ZPL is determined empirically in order for the lineshape to approximate the experimental lineshape. A measure of the extent of atomic structure change due to excitation is represented by the quantity ΔQ that is defined by the formula

$$\Delta Q^2 = \sum_{ai} m_a (R_{e,ai} - R_{g,ai})^2, \quad (2)$$

where a enumerates the atoms, $i = x, y, z$, m_a is the atomic mass of species a , and $R_{g/e,ai}$ is the position of atom a in the ground/excited state, respectively.

After considering a number of potential defects (including the defects in Ref. 21 as well as some of those defects in charged states) (details of these defects are presented in the [supplementary material](#)), we find that the observed emission is consistent with the negatively-charged nitrogen anti-site defect ($V_N N_B^{-1}$). The inset of Fig. 4(a) displays the geometry of this defect.

We compare between the shape and intensity of the calculated and observed phonon side bands in order to unravel the possible atomic structure of the defect site. Emission observed in the current experiment shows very little intensity to phonon processes, as is common in many other observations. This is quite unusual, and significantly nearly all potential defects studied theoretically²¹ have large Huang–Rhys factors and hence large phonon side bands. As demonstrated recently, calculating excitation energies with DFT is problematic. The PBE functional⁴¹ used here predicts a bandgap of 4.7 eV for bulk hBN, where the experimental value is 6 eV. The

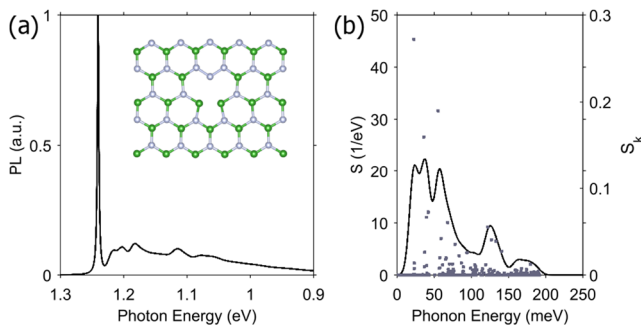


FIG. 4. For the $V_N N_B^{-1}$ defect, (a) the theoretical PL lineshapes, showing the ground state structure of the defect in the inset, and (b) the set of partial HR factors, S_k (displayed as square-shaped points) and the approximate partial HR function, $S(\hbar\omega)$ (displayed as solid curves). In the defect structure in (a), the white spheres represent nitrogen atoms and the green spheres boron atoms.

HSE06 functional⁴² reproduces the experimental value. The excited state energies for the neutral nitrogen anti-site defects are 0.4 eV smaller using the PBE functional compared with HSE06.⁴³ However, despite its ability to reproduce bandgaps, the HSE06 functional is questionable for excited states, particularly where these involve states with multi-reference character. Comparison with high level *ab initio* calculations shows differences of up to 1 eV.⁴⁴ Details of the modeling are presented in the [supplementary material](#).

The $V_N N_B^{-1}$ defect has a low HR factor of 1.61 and a calculated ZPL energy of 1.13 eV, which is consistent with the experimentally observed PL peak at 1.24 eV (998 nm). The defect's predicted PL lineshape is displayed in [Fig. 4](#), and the partial HR factors and the partial HR function are shown in [Fig. 4\(b\)](#). These functions are described in the [supplementary material](#).

The PL lineshape has a significant low-energy phonon side-band, unlike the situation in the visible-light PL spectra.²¹ The structure of the phonon side-band can be understood in light of [Fig. 4\(b\)](#). The square-shaped points in this figure are the partial HR factors, and those factors with the largest magnitude have phonon energies in the range 0 meV–50 meV. For this reason, the phonon side-band is close to the ZPL point.

V. DISCUSSION

In this letter, we show PL emission in the NIR from hBN, where the PL wavelength is consistent with being emitted by the negatively charged nitrogen anti-site lattice defect ($V_N N_B^{-1}$) (PL at 1.24 eV or 998 nm). The emission displays sub-Poissonian photon statistics [$g^{(2)}(0) < 1$] that demonstrates its non-classical nature; indeed, the photon statistics of the emission are consistent with SPE along with a high background of classical light. As we consider this background light to likely originate from other PL-emitting defects in hBN, future work will focus on suppressing this background PL in order to improve the purity of SPE. In fact, it was recently discovered that the irradiation of an hBN sample with a He^+ focused ion beam (FIB) causes a dramatic reduction in background PL [even to the point of reducing the $g^{(2)}(0)$ from above to below 0.5].³² Thus future work could apply He^+ FIB to confirm the $V_N N_B^{-1}$ lattice defect's

single photon emitter nature. In addition, the novel fabrication method of using a scanning tunneling microscope tip to position individual lattice defects could be used in future studies to analyze the PL from an individual defect and thereby confirm its SPS nature.⁴⁵

In summary, we have presented the first observation of a sub-Poissonian emission in the NIR in hBN, with a second-order coherence value of $g^{(2)}(0) = 0.6$. The emission was centered at 1.24 eV (998 nm) with an emitter lifetime of $\tau_{1.24 \text{ eV}} = 3.2$ ns. We attribute this emission to the negatively charged nitrogen anti-site defect. These results indicate the potential for hBN as a platform for single photon generation in the NIR.

SUPPLEMENTARY MATERIAL

See the [supplementary material](#) for details of the sample fabrication, experimental characterization, and the theoretical method.

AUTHORS' CONTRIBUTIONS

R.C. and L.M. contributed equally to this work.

ACKNOWLEDGMENTS

The authors thank Mr. Mihai Costache for LabVIEW support. The computational work was undertaken with the assistance of resources and services from the National Computational Infrastructure (NCI), which is supported by the Australian Government, and was supported by resources provided by the Pawsey Supercomputing Centre with funding from the Australian Government and the Government of Western Australia.

We acknowledge financial support from the School of Physics, the University of Sydney, and the experimental facilities therein.

DATA AVAILABILITY

The data that support the findings of this study are available from the corresponding author upon reasonable request.

REFERENCES

- M. Fox, *Quantum Optics: An Introduction* (OUP Oxford, 2006), Vol. 15.
- H. J. Kimble, "The quantum internet," *Nature* **453**, 1023–1030 (2008).
- J. B. Spring, B. J. Metcalf, P. C. Humphreys, W. S. Kolthammer, X.-M. Jin, M. Barbieri, A. Datta, N. Thomas-Peter, N. K. Langford, D. Kundys, J. C. Gates, B. J. Smith, P. G. R. Smith, and I. A. Walmsley, "Boson sampling on a photonic chip," *Science* **339**, 798 (2012).
- V. Giovannetti, S. Lloyd, and L. Maccone, "Advances in quantum metrology," *Nat. Photonics* **5**, 222 (2011).
- A. Peruzzo, M. Lobino, J. C. F. Matthews, N. Matsuda, A. Politi, K. Poulios, X.-Q. Zhou, Y. Lahini, N. Ismail, K. Wörhoff, Y. Bromberg, Y. Silberberg, M. G. Thompson, and J. L. O'Brien, "Quantum walks of correlated photons," *Science* **329**, 1500–1503 (2010).
- I. Aharonovich, D. Englund, and M. Toth, "Solid-state single-photon emitters," *Nat. Photonics* **10**, 631 (2016).
- M. D. Eisaman, J. Fan, A. Migdall, and S. V. Polyakov, "Invited review article: Single-photon sources and detectors," *Rev. Sci. Instrum.* **82**, 071101 (2011).

- ⁸T. Miyazawa, K. Takemoto, Y. Sakuma, S. Hirose, T. Usuki, N. Yokoyama, M. Takatsu, and Y. Arakawa, "Single-photon generation in the 1.55- μm optical-fiber band from an InAs/InP quantum dot," *Jpn. J. Appl. Phys., Part 2* **44**, L620 (2005).
- ⁹P. Senellart, G. Solomon, and A. White, "High-performance semiconductor quantum-dot single-photon sources," *Nat. Nanotechnol.* **12**, 1026 (2017).
- ¹⁰N. Somaschi, V. Giesz, L. De Santis, J. C. Loredó, M. P. Almeida, G. Hornecker, S. L. Portalupi, T. Grange, C. Antón, J. Demory, C. Gómez, I. Sagnes, N. D. Lanzillotti-Kimura, A. Lemaître, A. Auffèves, A. G. White, L. Lanco, and P. Senellart, "Near-optimal single-photon sources in the solid state," *Nat. Photonics* **10**, 340 (2016).
- ¹¹X. Ding, Y. He, Z.-C. Duan, N. Gregersen, M.-C. Chen, S. Unsleber, S. Maier, C. Schneider, M. Kamp, S. Höfling, C.-Y. Lu, and J.-W. Pan, "On-demand single photons with high extraction efficiency and near-unity indistinguishability from a resonantly driven quantum dot in a micropillar," *Phys. Rev. Lett.* **116**, 020401 (2016).
- ¹²Y. Piao, B. Meany, L. R. Powell, N. Valley, H. Kwon, G. C. Schatz, and Y. Wang, "Brightening of carbon nanotube photoluminescence through the incorporation of sp^3 defects," *Nat. Chem.* **5**, 840 (2013).
- ¹³A. Jeantet, Y. Chassagneux, C. Raynaud, P. Roussignol, J. Lauret, B. Besga, J. Estève, J. Reichel, and C. Voisin, "Widely tunable single-photon source from a carbon nanotube in the purcell regime," *Phys. Rev. Lett.* **116**, 247402 (2016).
- ¹⁴S. Khasminkaya, F. Pyatkov, K. Słowik, S. Ferrari, O. Kahl, V. Kovalyuk, P. Rath, A. Vetter, F. Hennrich, M. M. Kappes, G. Gol'tsman, A. Korneev, C. Rockstuhl, R. Krupke, and W. H. P. Pernice, "Fully integrated quantum photonic circuit with an electrically driven light source," *Nat. Photonics* **10**, 727 (2016).
- ¹⁵Y. Zhou, Z. Wang, A. Rasmita, S. Kim, A. Berhane, Z. Bodrog, G. Adamo, A. Gali, I. Aharonovich, and W.-b. Gao, "Room temperature solid-state quantum emitters in the telecom range," *Sci. Adv.* **4**, eaar3580 (2018).
- ¹⁶X. He, N. F. Hartmann, X. Ma, Y. Kim, R. Ihly, J. L. Blackburn, W. Gao, J. Kono, Y. Yomogida, A. Hirano, T. Tanaka, H. Kataura, H. Htoon, and S. K. Doorn, "Tunable room-temperature single-photon emission at telecom wavelengths from sp^3 defects in carbon nanotubes," *Nat. Photonics* **11**, 577 (2017).
- ¹⁷M. Zheng, "Sorting carbon nanotubes," *Top. Curr. Chem.* **375**, 13 (2017).
- ¹⁸J. D. Caldwell, I. Aharonovich, G. Cassabois, J. H. Edgar, B. Gil, and D. N. Basov, "Photonics with hexagonal boron nitride," *Nat. Rev. Mater.* **4**, 552–567 (2019).
- ¹⁹P. Tonndorf, R. Schmidt, R. Schneider, J. Kern, M. Buscema, G. A. Steele, A. Castellanos-Gomez, H. S. J. van der Zant, S. M. de Vasconcellos, and R. Bratschkitsch, "Single-photon emission from localized excitons in an atomically thin semiconductor," *Optica* **2**, 347–352 (2015).
- ²⁰T. T. Tran, K. Bray, M. J. Ford, M. Toth, and I. Aharonovich, "Quantum emission from hexagonal boron nitride monolayers," *Nat. Nanotechnol.* **11**, 37 (2016).
- ²¹S. A. Tawfik, S. Ali, M. Fronzi, M. Kianinia, T. T. Tran, C. Stampfl, I. Aharonovich, M. Toth, and M. J. Ford, "First-principles investigation of quantum emission from hBN defects," *Nanoscale* **9**, 13575–13582 (2017).
- ²²A. Sajid, M. J. Ford, and J. R. Reimers, "Single-photon emitters in hexagonal boron nitride: A review of progress," *Rep. Prog. Phys.* **83**, 044501 (2020).
- ²³T. T. Tran, C. Elbadawi, D. Totonjian, C. J. Lobo, G. Grosso, H. Moon, D. R. Englund, M. J. Ford, I. Aharonovich, and M. Toth, "Robust multicolor single photon emission from point defects in hexagonal boron nitride," *ACS Nano* **10**, 7331–7338 (2016).
- ²⁴R. Bourrellier, S. Meuret, A. Tararan, O. Stéphan, M. Kociak, L. H. G. Tizei, and A. Zobelli, "Bright UV single photon emission at point defects in *h*-BN," *Nano Lett.* **16**, 4317–4321 (2016).
- ²⁵T. Vogl, Y. Lu, and P. K. Lam, "Room temperature single photon source using fiber-integrated hexagonal boron nitride," *J. Phys. D: Appl. Phys.* **50**, 295101 (2017).
- ²⁶T. T. Tran, D. Wang, Z.-Q. Xu, A. Yang, M. Toth, T. W. Odom, and I. Aharonovich, "Deterministic coupling of quantum emitters in 2D materials to plasmonic nanocavity arrays," *Nano Lett.* **17**, 2634–2639 (2017).
- ²⁷X. Li, R. A. Scully, K. Shayan, Y. Luo, and S. Strauf, "Near-unity light collection efficiency from quantum emitters in boron nitride by coupling to metallo-dielectric antennas," *ACS Nano* **13**, 6992–6997 (2019).
- ²⁸M. Toth and I. Aharonovich, "Single photon sources in atomically thin materials," *Annu. Rev. Phys. Chem.* **70**, 123–142 (2019).
- ²⁹D. Wong, J. Velasco, Jr., L. Ju, J. Lee, S. Kahn, H.-Z. Tsai, C. Germany, T. Taniguchi, K. Watanabe, A. Zettl, F. Wang, and M. F. Crommie, "Characterization and manipulation of individual defects in insulating hexagonal boron nitride using scanning tunnelling microscopy," *Nat. Nanotechnol.* **10**, 949–953 (2015).
- ³⁰M. Nguyen, S. Kim, T. T. Tran, Z.-Q. Xu, M. Kianinia, M. Toth, and I. Aharonovich, "Nanoassembly of quantum emitters in hexagonal boron nitride and gold nanospheres," *Nanoscale* **10**, 2267–2274 (2018).
- ³¹J. Ziegler, R. Klais, A. Blaikie, D. Miller, V. R. Horowitz, and B. J. Alemán, "Deterministic quantum emitter formation in hexagonal boron nitride via controlled edge creation," *Nano Lett.* **19**, 2121–2127 (2019).
- ³²G. Grosso, H. Moon, B. Lienhard, S. Ali, D. K. Efetov, M. M. Furchi, P. Jarillo-Herrero, M. J. Ford, I. Aharonovich, and D. Englund, "Tunable and high-purity room temperature single-photon emission from atomic defects in hexagonal boron nitride," *Nat. Commun.* **8**, 705 (2017).
- ³³N. Mendelson, Z.-Q. Xu, T. T. Tran, M. Kianinia, J. Scott, C. Bradac, I. Aharonovich, and M. Toth, "Engineering and tuning of quantum emitters in few-layer hexagonal boron nitride," *ACS Nano* **13**, 3132–3140 (2019).
- ³⁴F. Hayee, L. Yu, J. L. Zhang, C. J. Ciccarino, M. Nguyen, A. F. Marshall, I. Aharonovich, J. Vučković, P. Narang, T. F. Heinz, and J. A. Dionne, "Revealing multiple classes of stable quantum emitters in hexagonal boron nitride with correlated optical and electron microscopy," *Nat. Mater.* **19**(5), 534–539 (2020).
- ³⁵A. Gottscholl, M. Kianinia, V. Soltamov, S. Orlinskii, G. Mamin, C. Bradac, C. Kasper, K. Krambrock, A. Sperlich, M. Toth, I. Aharonovich, and V. Dyakonov, "Initialization and read-out of intrinsic spin defects in a van der Waals crystal at room temperature," *Nat. Mater.* **19**, 540–545 (2020).
- ³⁶K. A. Fischer, K. Müller, K. G. Lagoudakis, and J. Vučković, "Dynamical modeling of pulsed two-photon interference," *New J. Phys.* **18**, 113053 (2016).
- ³⁷F. T. Rabouw, N. M. B. Cogan, A. C. Berends, W. v. d. Stam, D. Vanmaekelbergh, A. F. Koenderink, T. D. Krauss, and C. d. M. Donega, "Non-blinking single-photon emitters in silica," *Sci. Rep.* **6**, 21187 (2016).
- ³⁸R. Kubo and Y. Toyozawa, "Application of the method of generating function to radiative and non-radiative transitions of a trapped electron in a crystal," *Prog. Theor. Phys.* **13**, 160–182 (1955).
- ³⁹A. Alkauskas, B. B. Buckley, D. D. Awschalom, and C. G. Van de Walle, "First-principles theory of the luminescence lineshape for the triplet transition in diamond NV centres," *New J. Phys.* **16**, 073026 (2014).
- ⁴⁰A. Alkauskas, J. L. Lyons, D. Steiauf, and C. G. Van de Walle, "First-principles calculations of luminescence spectrum line shapes for defects in semiconductors: The example of GaN and ZnO," *Phys. Rev. Lett.* **109**, 267401 (2012).
- ⁴¹J. P. Perdew, K. Burke, and M. Ernzerhof, "Generalized gradient approximation made simple," *Phys. Rev. Lett.* **77**, 3865–3868 (1996).
- ⁴²J. Heyd, G. E. Scuseria, and M. Ernzerhof, "Hybrid functionals based on a screened Coulomb potential," *J. Chem. Phys.* **118**, 8207–8215 (2003).
- ⁴³M. Abdi, J.-P. Chou, A. Gali, and M. B. Plenio, "Color centers in hexagonal boron nitride monolayers: A group theory and ab initio analysis," *ACS Photonics* **5**, 1967–1976 (2018).
- ⁴⁴J. R. Reimers, A. Sajid, R. Kobayashi, and M. J. Ford, "Understanding and calibrating density-functional-theory calculations describing the energy and spectroscopy of defect sites in hexagonal boron nitride," *J. Chem. Theory Comput.* **14**, 1602–1613 (2018).
- ⁴⁵Y.-C. Chen, T. Cao, C. Chen, Z. Pedramrazi, D. Haberer, D. G. de Oteyza, F. R. Fischer, S. G. Louie, and M. F. Crommie, "Molecular bandgap engineering of bottom-up synthesized graphene nanoribbon heterojunctions," *Nat. Nanotechnol.* **10**, 156 (2015).